Journal of Computational Physics 228 (2009) 7197–7214

Contents lists available at ScienceDirect

Journal of Computational Physics

journal homepage: www.elsevier.com/locate/jcp

Navier–Stokes spectral solver in a sphere

F. Auteri *, L. Quartapelle

Politecnico di Milano, Dipartimento di Ingegneria Aerospaziale, Via La Masa 34, 20156 Milano, Italy

ARTICLE INFO

Article history:
Received 25 November 2008
Received in revised form 27 April 2009
Accepted 16 June 2009
Available online 23 June 2009

Keywords:
Navier–Stokes equations
Spectral methods
Projection methods
Spherical coordinates

ABSTRACT

The paper presents the first implementation of a primitive variable spectral method for calculating viscous flows inside a sphere. A variational formulation of the Navier–Stokes equations is adopted using a fractional-step time discretization with the classical second-order backward difference scheme combined with explicit extrapolation of the nonlinear term. The resulting scalar and vector elliptic equations are solved by means of the direct spectral solvers developed recently by the authors. The spectral matrices for radial operators are characterized by a minimal sparsity – diagonal stiffness and tridiagonal mass matrix. Closed-form expressions of their nonzero elements are provided here for the first time, showing that the condition number of the relevant matrices grows as the second power of the truncation order. A new spectral elliptic solver for the velocity unknown in spherical coordinates is also described that includes implicitly the Coriolis force in a rotating frame, but requires a minimal coupling between the modal velocity components in the Fourier space. The numerical tests confirm that the proposed method achieves spectral accuracy and ensures infinite differentiability to all orders of the numerical solution, by construction. These results indicate that the new primitive variable spectral solver is an effective alternative to the spectral method recently proposed by Kida and Nakayama, where the velocity field is represented in terms of poloidal and toroidal functions.

1. Introduction

A central difficulty in the spectral simulation of flows inside a sphere comes from the singularity of the spherical coordinate system at the origin. A mathematically inappropriate treatment of this aspect may compromise the differentiability to any order of the solution and therefore also prevent the achievement of spectral accuracy, see, *e.g.*, [1], and the references therein. In a recent paper [2] spectral algorithms for the solution of elliptic equations in a spherical domain have been proposed employing a new basis built on Jacobi polynomials for the representation of the radial dependence up to the sphere centre. One key element of these direct spherical elliptic solvers is that the shape of basis functions for scalar or vector unknowns in the radial direction depends on the angular mode considered. Notably, their number decreases with the latitudinal modal index.

The basic idea underlying these new spectral elliptic solvers is that, as fewer associated Legendre functions are needed for the approximate representation of latitudinal variations of higher Fourier modes over a spherical surface, also fewer Jacobi polynomials are needed for the resolution of the radial structure of higher latitudinal modes inside a sphere. As a consequence of the use of the new Jacobi basis, the elliptic solvers do not face any difficulty with the sphere centre much in the same manner the spherical harmonics suffer no pole problem, and in fact the expected spectral convergence has been actually achieved in all computational tests [2]. Moreover, the new basis leads to matrices for radial operators characterized

* Corresponding author. Tel.: +39 02 2399 8046; fax: +39 02 2399 8334.
E-mail address: auteri@aero.polimi.it (F. Auteri).

0021-9991/$ - see front matter © 2009 Elsevier Inc. All rights reserved.
doi:10.1016/j.jcp.2009.06.016

by a very nice sparsity: for any latitudinal mode, the stiffness matrix is diagonal and the mass matrix is tridiagonal. Remarkably enough, all their nonzero elements can be given in closed form, as unveiled for the first time in the present paper. The condition number of the matrices associated with the radial part of Helmholtz operator grows as the second power of the degree of the basis, which represents a major numerical advantage in the context of spectral methods. Finally, the basis functions can be divided in two subsets: one subset is zero on the boundary, the other subset is not and can be employed to simply fulfill Dirichlet boundary conditions.

Since the pioneering work of Orszag [3] several authors have contributed to develop spectral methods for solving the incompressible Navier–Stokes equations in spherical domains. Without pretending to give an exhaustive account of all these efforts, we mention only some of the most representative examples. Marcus and Tuckerman formulated a pseudospectral method using the influence matrix technique to investigate spherical Couette flow [4,5]. The first successful attempt to use a spectral approximation to the incompressible Navier–Stokes equations in spherical coordinates including the origin was described in the paper by Stanaway et al. [6] and applied to simulate an axisymmetric vortex ring. Jacobi polynomials were introduced for expanding the solutions in an unbounded domain, with the radial variable mapped from the semi-infinite interval to a finite range. The method employs a divergenceless spectral (quasi-orthogonal) basis for the velocity field with the pressure variable eliminated from the problem, following the ideas introduced by Moser et al. to compute fully 3D flows within plane or cylindrical walls [7] and later employed by Dumas and Leonard inside a spherical gap [8]. Tau-Chebyshev discretizations were proposed by Quartapelle and Verri in conjunction with the idea of integral conditions for pressure to solve the incompressible equation within a spherical gap and inside a sphere [9]. Shen and Wang simulated atmospheric flows [10] by means of a Galerkin spectral method employing the direct spherical solver developed by Shen in [11]. Finally, spectral methods have been recently proposed by Mininni and Montgomery employing Chandrasekhar–Kendall eigenfunctions [12], by Guo and Huang using Jacobi polynomials and spherical harmonics [13] and by Kida and Nakayama using poloidal and toroidal functions [14]. The method of the last reference employs a radial discretization decreasing with the latitudinal modal index, as the spectral elliptic solvers of [2]. Several examples of simulations of rotating flows in spherical geometries can be found in the monograph of Egbers and Pfister [15].

The aim of the present paper is to develop a primitive-variable spectral method for simulating viscous incompressible flows inside a sphere employing the aforementioned direct elliptic solvers. When the Navier–Stokes equations are tackled by a spectral method a number of additional aspects must be addressed. In particular, we develop a Galerkin incremental projection method with a second-order BDF time integration of the momentum equation and linear extrapolation of the advection term, extending our previous efforts for flows in Cartesian regions in 2D [16] and 3D [17] to a spherical domain.

The paper is organized as follows. In Section 2, the mathematical problem is stated and the basic elements of the second-order incremental fractional-step method are provided. In Section 3, we briefly outline the spectral elliptic solvers. In Section 4, the procedures for evaluating the gradient, the divergence and the nonlinear term in weak form are described. Section 5 addresses the Navier–Stokes problem in a rotating frame. Section 6 is devoted to numerical tests for flows in inertial and noninertial frames, some concluding remarks follow.

2. Navier–Stokes equations and projection method

This paper deals with the motion of a viscous fluid of uniform density inside a sphere Ω of radius a, which is governed by the incompressible Navier–Stokes equations

$$\begin{cases} \frac{\partial \boldsymbol{u}}{\partial t} + (\boldsymbol{u}\cdot\nabla)\boldsymbol{u} - \nu\nabla^2\boldsymbol{u} + \nabla p = \boldsymbol{f}(\boldsymbol{r},t), \quad \nabla\cdot\boldsymbol{u} = 0, \\ \boldsymbol{u}_{|\partial\Omega} = \boldsymbol{b}, \quad \boldsymbol{u}_{|t=0} = \boldsymbol{u}_0, \end{cases} \tag{2.1}$$

where $\boldsymbol{u}$ is the velocity, $p = P/\bar{\rho}$ is the pressure per unit density of the fluid, ν is the kinematic viscosity and $\boldsymbol{f}(\boldsymbol{r},t)$ is an external force field (per unit mass) possibly acting on the fluid, for example the gravitational field. In the problem above, $\boldsymbol{b}(\boldsymbol{r}_{\partial\Omega},t)$ represents the velocity prescribed on the boundary, satisfying $\int_{\partial\Omega}\boldsymbol{n}\cdot\boldsymbol{b} = 0$, and $\boldsymbol{u}_0(\boldsymbol{r})$ is the initial solenoidal velocity field.

The Navier–Stokes problem (2.1) is solved by means of the second-order BDF incremental fractional-step projection method described in [18,19] in the context of a finite element spatial discretization. In view of the spectral discretization of interest here, we assume an implicit treatment for the viscous term and an explicit account for the nonlinear term, with a linear extrapolation of the velocity field at the new time level. As a consequence, the method will be only conditionally stable, with time-step size limited by a suitable stability restriction.

As well known, the fractional-step approach is based on splitting the time advancement of the momentum equation in two distinct phases or sub-steps. The first sub-step consists in the following viscous problem for the vector unknown $\boldsymbol{u}^{k+1}$:

$$\begin{cases} \frac{3\boldsymbol{u}^{k+1}-4\boldsymbol{u}^{k}+\boldsymbol{u}^{k-1}}{2\Delta t} - \nu\nabla^2\boldsymbol{u}^{k+1} = \boldsymbol{f}^{\,k+1} - \nabla p^{k}_{\star} - (\boldsymbol{u}^{k+1}_{\star}\cdot\nabla)\boldsymbol{u}^{k+1}_{\star}, \\ \boldsymbol{u}^{k+1}_{|\partial\Omega} = \boldsymbol{b}^{k+1}, \end{cases} \tag{2.2}$$

where $\boldsymbol{f}^{k+1} = \boldsymbol{f}(\boldsymbol{r},t_{k+1})$ and $\boldsymbol{b}^{k+1} = \boldsymbol{b}(\boldsymbol{r}_{\partial\Omega},t_{k+1})$. Moreover, the extrapolated velocity and pressure are defined respectively by

$$\boldsymbol{u}^{k+1}_{\star} = \begin{cases} \boldsymbol{u}_0 & \text{for } k = 0 \\ 2\boldsymbol{u}^{k} - \boldsymbol{u}^{k-1} & \text{for } k \geqslant 1 \end{cases} \tag{2.3}$$

and

$$p_\star^k = \begin{cases} p_0 & \text{for } k=0 \\ 3p^1 - 2p_0 & \text{for } k=1 \\ \frac{1}{6}(14p^2 - 11p^1 + 3p_0) & \text{for } k=2 \\ \frac{1}{3}(7p^k - 5p^{k-1} + p^{k-2}) & \text{for } k \geqslant 3 \end{cases} \tag{2.4}$$

where p_0 is an initial pressure field which must be provided or envisaged insofar as the incremental method is employed since the first time step.

The second sub-step consists in projecting $\boldsymbol{u}^{k+1}$ onto the space of the divergenceless vector fields that are tangent to the boundary $\partial\Omega$. This step can be formulated as the following elliptic problem

$$\begin{cases} -\nabla^2(p^{k+1} - p^k) = -\frac{3}{2\Delta t}\,\boldsymbol{\nabla}\cdot\boldsymbol{u}^{k+1}, \\ \partial_n(p^{k+1} - p^k)|_{\partial\Omega} = 0. \end{cases} \tag{2.5}$$

Therefore, the projection step assumes the form of a Poisson equation for the pressure increment $p^{k+1} - p^k$, supplemented by homogeneous Neumann boundary condition. Note that no pressure condition is prescribed in the original time-continuous problem (2.1) and that the Neumann condition in (2.5) results from Ladyzenskaya's orthogonality theorem once the incompressible step is formulated as a Poisson equation for pressure.

The time integration schemes in problems (2.2) and (2.5) are both second order accurate. The convergence in time of the method (2.2)–(2.4) and (2.5) has been demonstrated by Guermond [20]. A review of projection methods is given by Guermond et al. [21].

3. Discretized equations in spherical coordinates

3.1. Helmholtz equation for velocity

At each viscous step one has to solve the vector Helmholtz equation in spherical coordinates (r,θ,ϕ)

$$(-\nabla^2 + \gamma)\boldsymbol{u} = \boldsymbol{f}(r,\theta,\phi), \tag{3.1}$$

with $\gamma \geqslant 0$ and $\boldsymbol{f}(r,\theta,\phi)$ a given source term, supplemented by the Dirichlet condition $\boldsymbol{u}(1,\theta,\phi) = \boldsymbol{b}(\theta,\phi)$, for $\partial p(1,\theta,\phi)/\partial r = 0$. The radial variable r has been made dimensionless by taking the radius a of the sphere as the reference length. The vector variable $\boldsymbol{u}$ is first expanded in a Fourier series, dropping the highest cosine component with $m = N$, to give

$$\boldsymbol{u}(r,\theta,\phi) = \boldsymbol{u}^0(r,\theta) + 2\sum_{m=1}^{N-1}[\boldsymbol{u}^m(r,\theta)\cos(m\phi) - \boldsymbol{u}^{-m}(r,\theta)\sin(m\phi)]. \tag{3.2}$$

The Fourier vector coefficients are $\boldsymbol{u}^m(r,\theta) = u_r^m(r,\theta)\,\hat{\boldsymbol{r}} + u_\theta^m(r,\theta)\,\hat{\boldsymbol{\theta}} + u_\phi^m(r,\theta)\,\hat{\boldsymbol{\phi}}$, with $\hat{\boldsymbol{r}}$, $\hat{\boldsymbol{\theta}}$ and $\hat{\boldsymbol{\phi}}$ denoting the unit vectors of the spherical coordinate system.

Written in the space of the Fourier coefficients, the operator representing the Laplace vector operator ∇^2 is

$$\boldsymbol{\partial}_m^2 = \begin{pmatrix} \partial_m^2 - \frac{2}{r^2} & -\frac{2}{r^2\sin\theta}\frac{\partial}{\partial\theta}(\sin\theta\,\ldots) & \frac{2m}{r^2\sin\theta} \\ \frac{2}{r^2}\frac{\partial}{\partial\theta} & \partial_m^2 - \frac{1}{r^2\sin^2\theta} & \frac{2m\cos\theta}{r^2\sin^2\theta} \\ \frac{2m}{r^2\sin\theta} & \frac{2m\cos\theta}{r^2\sin^2\theta} & \partial_m^2 - \frac{1}{r^2\sin^2\theta} \end{pmatrix}, \tag{3.3}$$

where the scalar operator ∂_m^2, with $m = 0,1,2,\ldots$, is defined by

$$\partial_m^2 \equiv \frac{1}{r^2}\frac{\partial}{\partial r}\left(r^2\frac{\partial}{\partial r}\right) + \frac{1}{r^2\sin\theta}\frac{\partial}{\partial\theta}\left(\sin\theta\frac{\partial}{\partial\theta}\right) - \frac{m^2}{r^2\sin^2\theta}. \tag{3.4}$$

The equation system for the coefficients of the m-th Fourier mode reads

$$(-\boldsymbol{\partial}_m^2 + \gamma)\begin{pmatrix} u_r^m \\ u_\theta^m \\ u_\phi^{-m} \end{pmatrix} = \begin{pmatrix} f_r^m(r,\theta) \\ f_\theta^m(r,\theta) \\ f_\phi^{-m}(r,\theta) \end{pmatrix}. \tag{3.5}$$

Thus, for $m \neq 0$ the three spherical components of the vector Fourier mode are coupled together, while for the first mode $m = 0$ only the first two components u_r^0 and u_θ^0 are coupled together.

Once the uncoupling technique described in [2] is applied, the new unknowns become u_1^m, u_2^m and u_3^m, and they are related to the former by the transformation

$$\begin{pmatrix} u_1^{m-1} \\ u_2^m \\ u_3^{m+1} \end{pmatrix} = \boldsymbol{\Theta} \begin{pmatrix} u_r^m \\ u_\theta^m \\ u_\phi^{-m} \end{pmatrix} = \frac{1}{\sqrt{2}} \begin{pmatrix} \sin\theta & \cos\theta & 1 \\ \sqrt{2}\cos\theta & -\sqrt{2}\sin\theta & 0 \\ \sin\theta & \cos\theta & -1 \end{pmatrix} \begin{pmatrix} u_r^m \\ u_\theta^m \\ u_\phi^{-m} \end{pmatrix}. \tag{3.6}$$

The transformation $\boldsymbol{\Theta}$ diagonalizes the matrix operator $\boldsymbol{\partial}_m^2$ in the sense that

$$\boldsymbol{\Theta}\,\boldsymbol{\partial}_m^2\,\boldsymbol{\Theta}^T = \begin{pmatrix} \partial_{m-1}^2 & 0 & 0 \\ 0 & \partial_m^2 & 0 \\ 0 & 0 & \partial_{m+1}^2 \end{pmatrix}. \tag{3.7}$$

The same transformation is applied to the right-hand side $\boldsymbol{f}$.

The solution of the equations for the m-th Fourier mode with $m \neq 0$ proceeds as follows: first, the transformation $\boldsymbol{\Theta}$ is applied to the Fourier coefficient $\boldsymbol{f}^m$ of the source term $\boldsymbol{f}$ of the Helmholtz equation, then the three uncoupled elliptic 2D equations are solved and finally the inverse transformation to the spherical components is performed. For $m = 0$ the solution procedure is the very same, but the transformation matrix $\boldsymbol{\Theta}$ and the diagonalized vector operator are replaced by

$$\boldsymbol{\Theta}_0 = \begin{pmatrix} \sin\theta & \cos\theta & 0 \\ \cos\theta & -\sin\theta & 0 \\ 0 & 0 & 1 \end{pmatrix} \quad \text{and} \quad \boldsymbol{\Theta}_0\,\boldsymbol{\partial}_0^2\,\boldsymbol{\Theta}_0 = \begin{pmatrix} \partial_1^2 & 0 & 0 \\ 0 & \partial_0^2 & 0 \\ 0 & 0 & \partial_1^2 \end{pmatrix}, \tag{3.8}$$

respectively. When acting on the full set of the Fourier expansion coefficients of a vector field, the pair of matrices $\boldsymbol{\Theta}$ and $\boldsymbol{\Theta}_0$ defines the operator Θ between the two representations of the vector mode:

$$\{\breve{\boldsymbol{u}}^m, m = 0, \pm 1, \ldots\} = \Theta\{\boldsymbol{u}^m, m = 0, \pm 1, \ldots\}, \tag{3.9}$$

where $\breve{\boldsymbol{u}}^m = (u_1^m, u_2^m, u_3^m)$ and $\boldsymbol{u}^m = (u_r^m, u_\theta^m, u_\phi^m)$.

3.2. Uncoupled scalar Dirichlet problem

The scalar elliptic equation for each of the three uncoupled velocity components u_χ^m, with $\chi = 1, 2, 3$, will be written as

$$(-\partial_m^2 + \gamma)u^m = f^m(r, \theta), \tag{3.10}$$

supplemented by the Dirichlet boundary condition $u^m(1, \theta) = b^m(\theta)$, for $0 \leqslant \theta \leqslant \pi$. The unknown variable $u^m(r, \theta)$ is then expanded in terms of the normalized associated Legendre functions $\widehat{P}_\ell^m(\cos\theta)$

$$u^m(r, \theta) = \sum_{\ell=|m|}^{N} u_\ell^m(r)\,\widehat{P}_\ell^{|m|}(\cos\theta), \quad -N + 1 \leqslant m \leqslant N - 1, \tag{3.11}$$

with the basis functions $\widehat{P}_\ell^m(z), z = \cos\theta$, related to the standard associated Legendre functions $P_\ell^m(z)$ by

$$\widehat{P}_\ell^m(z) \equiv \sqrt{\frac{2\ell + 1}{2}\frac{(\ell - m)!}{(\ell + m)!}}\,P_\ell^m(z). \tag{3.12}$$

The elliptic Eq. (3.10), once expressed in weak form, reduces to the following set of equations for the modal unknowns $u_\ell^m(r)$:

$$\int_0^1 v\left\{-\frac{d}{dr}\left(r^2\frac{du_\ell^m}{dr}\right) + [\ell(\ell + 1) + \gamma r^2]\,u_\ell^m\right\}dr = \int_0^1 r^2\,v(r) f_\ell^m(r)\,dr, \tag{3.13}$$

where $v(r)$ is a suitable weighting function and

$$f_\ell^m(r) = \int_0^\pi f^m(r, \theta)\,\widehat{P}_\ell^{|m|}(\cos\theta)\,\sin\theta\,d\theta. \tag{3.14}$$

Eq. (3.13) is supplemented by the boundary condition $u_\ell^m(1) = b_\ell^m$.

Finally, the modal unknown $u_\ell^m(r)$ is expanded as follows

$$u_\ell^m(r) = \sum_{i=0}^{N-\ell} u_{i;\ell}^m\,B_i^\ell(r), \tag{3.15}$$

exploiting the Jacobi polynomial basis [2]

$$B_i^\ell(r) \equiv Q_i^\ell(2r^2 - 1) = \begin{cases} r^\ell & \text{for } i = 0, \\ (1 - r^2)r^\ell P_{i-1}^{(1,\ell+\frac{1}{2})}(2r^2 - 1) & \text{for } i \geqslant 1. \end{cases} \tag{3.16}$$

Thus the complete spectral expansion of the Fourier component $u^m(r,\theta)$ of uncoupled velocity is given by the relation

$$u^m(r,\theta) = \sum_{\ell=|m|}^{N} \left[\sum_{i=0}^{N-\ell} u_{i;\ell}^m B_i^\ell(r) \right] \widehat{P}_\ell^{|m|}(\cos\theta). \tag{3.17}$$

The corresponding spectral version of the weak Eq. (3.13) for the modal unknowns $u_\ell^m(r)$ consists in an algebraic system of equations, described thoroughly in [2]. After integrating by parts in (3.13), the linear system assumes the form

$$(D_{[\ell]} + \gamma M_{[\ell]}) u_{[\ell]}^m = f_{[\ell]}^m, \tag{3.18}$$

where $u_{[\ell]}^m = \{u_{i;\ell}^m,\ i = 0,1,\ldots,N-\ell\}$ and the matrices $D_{[\ell]}$ and $M_{[\ell]}$ have elements defined by (using the mapped variable $s = 2r^2 - 1$)

$$D_{[\ell]\,i,i'} = \int_{-1}^{1} \left\{ 4\left(\frac{1+s}{2}\right)^{\frac{3}{2}} \frac{dQ_i^\ell(s)}{ds} \frac{dQ_{i'}^\ell(s)}{ds} + \frac{\ell(\ell+1)}{4} \left(\frac{1+s}{2}\right)^{-\frac{1}{2}} Q_i^\ell(s) Q_{i'}^\ell(s) \right\} ds,\ 0 \leqslant (i,i') \leqslant N-\ell, \tag{3.19}$$

$$M_{[\ell]\,i,i'} = \frac{1}{4} \int_{-1}^{1} \left(\frac{1+s}{2}\right)^{\frac{1}{2}} Q_i^\ell(s) Q_{i'}^\ell(s)\, ds, \quad 0 \leqslant (i,i') \leqslant N-\ell. \tag{3.20}$$

The order of a matrix with subscript $_{[\ell]}$ is $N-\ell+1$, and is therefore $(N+1), N, (N-1), \ldots, 2, 1$ for $\ell = 0, 1, 2, \ldots, N$,

Matrix $D_{[\ell]}$ is diagonal while matrix $M_{[\ell]}$ is symmetric tridiagonal [2], their nonzero elements are shown here for the first time to be

$$D_{[\ell]\,i,i} = \begin{cases} \ell & \text{for } i = 0, \\ \frac{2i^2}{2i+\ell+\frac{1}{2}} & \text{for } i \geqslant 1 \end{cases} \tag{3.21}$$

and

$$\begin{aligned} M_{[\ell]\,i,i} &= \begin{cases} \frac{1}{2\ell+3} & \text{for } i = 0, \\ \frac{i^2}{\left(2i+\ell-\frac{1}{2}\right)\left(2i+\ell+\frac{1}{2}\right)\left(2i+\ell+\frac{3}{2}\right)} & \text{for } i \geqslant 1, \end{cases} \\ M_{[\ell]\,i,i+1} &= \begin{cases} \frac{2}{(2\ell+3)(2\ell+5)} & \text{for } i = 0, \\ \frac{-i(i+1)}{2\left(2i+\ell+\frac{1}{2}\right)\left(2i+\ell+\frac{3}{2}\right)\left(2i+\ell+\frac{5}{2}\right)} & \text{for } i \geqslant 1. \end{cases} \end{aligned} \tag{3.22}$$

The tridiagonal character of the mass matrix $M_{[\ell]}$ follows from the definition of the basis functions $Q_i^\ell(s)$ and from the orthogonality of the Jacobi polynomials $P_i^{(1,\beta)}(s)$ and the nonzero elements of the mass matrix are obtained using this relation. The diagonal character of the stiffness matrix $D_{[\ell]}$ can be proved[1] starting from Eq. (3.13) and using the Jacobi orthogonality and differential equations.

The components of the right-hand side of linear system (3.18) are defined by

$$f_{[\ell]i}^m = \frac{1}{4} \int_{-1}^{1} \left(\frac{1+s}{2}\right)^{\frac{1}{2}} Q_i^\ell(s) f_\ell^m\left(\left(\frac{1+s}{2}\right)^{\frac{1}{2}}\right) ds + \langle \text{b.t.} \rangle, \tag{3.23}$$

where $\langle$b.t.$\rangle$ denotes a boundary contribution that is irrelevant under Dirichlet boundary conditions.

In the uncoupled algorithm, the Dirichlet boundary condition is taken into account by means of a lifting, which consists in relieving the nonzero boundary value by an arbitrary function and obtaining a problem supplemented by a homogeneous boundary condition. This is achieved by reducing the matrices of each scalar spectral component to their lifted counterparts, which are denoted by

$$\mathsf{A}_{[\ell]} = \mathsf{D}_{[\ell]} + \gamma \mathsf{M}_{[\ell]}, \tag{3.24}$$

where $\mathsf{A}_{[\ell]}, \mathsf{D}_{[\ell]}$ and $\mathsf{M}_{[\ell]}$ denote the matrices of the lifted problem. Thus, the independent equations for the uncoupled components of the vector unknown will be

$$\mathsf{A}_{[\ell]}\, \mathsf{u}_{[\ell]}^{m-2+\chi:\chi} = \mathsf{g}_{[\ell]}^{m-2+\chi:\chi}, \quad \chi = 1,2,3, \tag{3.25}$$

where $\mathsf{g}_{[\ell]}^{m:\chi} = \mathsf{f}_{[\ell]}^{m:\chi} - A_{[\ell]}^s\, b_{[\ell]}^{m:\chi}$, with $\chi = 1,2,3$. Here $\mathsf{u}_{[\ell]}^{m:\chi}$, with $\chi = 1,2,3$, denote the vector unknown of the lifted problem, $\mathsf{g}_{[\ell]}^{m:\chi}$ is its right-hand side after including the effect of the nonzero boundary value, and $b_{[\ell]}^{m:\chi}$ are the expansion coefficients of the velocity boundary value $\boldsymbol{b}$ on the sphere. Moreover, the original matrix $\mathsf{A}_{[\ell]}$ before the lifting has been partitioned into an

[1] P. W. Livermore, private communication, 2008.

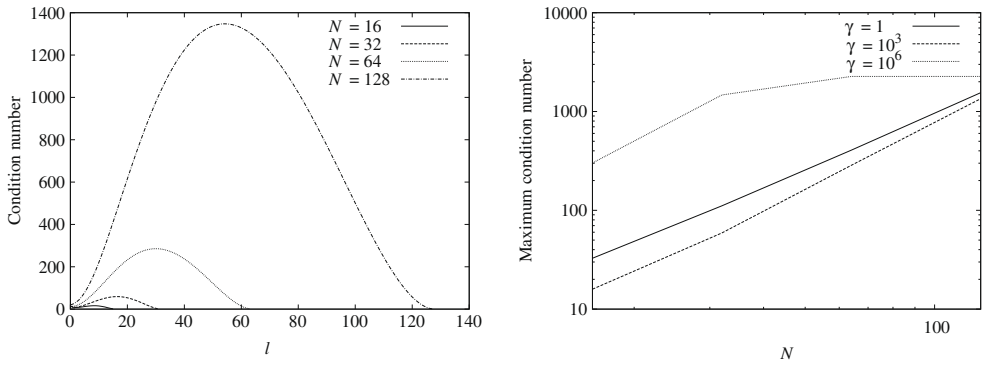

Fig. 1. Condition numbers of matrices (3.24) of the Dirichlet problem. Left: distribution of the condition number with the latitudinal modal index ℓ for different truncations and $\gamma = 1000$. Right: maximum condition number as a function of the truncation N of the radial expansion for different values of γ.

"internal" component $\mathsf{A}_{[\ell]}$, with elements $a_{[\ell]i,i'}$ such that $1 \leqslant (i,i') \leqslant N-\ell$, and a "surface" component represented by its first column

$$A^s_{[\ell]} = \{a_{[\ell]i,0},\ i = 1,2,\ldots,N-\ell\}, \tag{3.26}$$

with the first diagonal element $a_{[\ell]0,0}$ eliminated.

In Fig. 1 we report the condition numbers of the matrices $\mathsf{A}_{[\ell]}$. The left plot shows the dependence of the condition number on the radial modal index ℓ for different truncations with $\gamma = 1000$. The maximum condition number is found to correspond to the intermediate wavelengths of the truncated radial expansion. The plot on the right gives the maximum condition number for different truncations and different γ values. For small and intermediate values the maximum condition number depends quadratically on the truncation N; thus the spectral matrices for the Dirichlet problem of the proposed basis have an optimal conditioning. At higher γ, for instance for $\gamma = 10^6$, the maximum condition number is higher for moderate truncation but reveals an increasingly weaker dependence on N.

3.3. Neumann problem for pressure

At each incompressible step one has to solve the Poisson equation $-\nabla^2 p = q(r,\theta,\phi)$, where the given source term $q(r,\theta,\phi)$ satisfies $\int q\, d\Omega = 0$, supplemented by the homogeneous Neumann condition $\partial p(1,\theta,\phi)/\partial r = 0$ on the spherical boundary. The Poisson–Neumann solver is thoroughly described in [2] and is briefly recalled here for convenience. The pressure field is given by the following complete expansion

$$p(r,\theta,\phi) = \sum_{\ell=0}^{N}\left[\sum_{i=0}^{N-\ell} p^0_{i;\ell}\, B^\ell_i(r)\right]\widehat{P}^0_\ell(\cos\theta) + 2\sum_{m=1}^{N-1}\left\{\sum_{\ell=m}^{N}\left[\sum_{i=0}^{N-\ell} p^{\pm m}_{i;\ell}\, B^\ell_i(r)\right]\widehat{P}^m_\ell(\cos\theta)\right\}\begin{matrix}\cos(m\phi)\\ -\sin(m\phi)\end{matrix} + p^N_{0;N}\, r^N \widehat{P}^N_N(\cos\theta)\,\cos(N\phi). \tag{3.27}$$

The superposed cosine and sine functions in the external summation correspond to the two signs in $\pm m$ involved by the Fourier sum over m. In expansion (3.27) the presence of the last term of the cosine component of order N and the absence of the coefficient 2 in front are driven by the FFTW package employed [22]. The total number of cosine and sine expansion coefficients for pressure is equal to $(N+1)(N+2)(2N+3)/6$.

The equation for $p^m(r,\theta)$, with $-N+1 \leqslant m \leqslant N$, is

$$(-\partial^2_m + \gamma)p^m = q^m(r,\theta), \tag{3.28}$$

and is supplemented by the derivative boundary condition $\partial p^m(1,\theta)/\partial r = 0$, for $0 \leqslant \theta \leqslant \pi$. $q^m(r,\theta)$ are the Fourier expansion coefficients of the source $q(r,\theta,\phi)$.

The pressure modal unknown $p^m_\ell(r)$ must satisfy the second order equation expressed in weak form as

$$\int_0^1 v\left[-\frac{d}{dr}\left(r^2\,\frac{dp^m_\ell}{dr}\right) + \ell(\ell+1)p^m_\ell\right]dr = \int_0^1 r^2\, v(r) q^m_\ell(r)\, dr, \tag{3.29}$$

and the derivative condition $dp^m_\ell(1)/dr = 0$, with $v(r)$ denoting a suitable weighting function. After integrating by parts and taking into account the natural boundary condition, the spectral approximation of the weak Eq. (3.29) leads to the fully diagonal linear system

$$D_{[\ell]} p^m_{[\ell]} = q^m_{[\ell]}. \tag{3.30}$$

where $p^m_{[\ell]} = \{p^m_{i;\ell},\ i = 0,1,\ldots,N-\ell\}$ and with matrix $D_{[\ell]}$ already defined in (3.21). Notice that the first diagonal matrix $D_{[\ell]}$ is singular in conformity with the singularity of the Neumann boundary value problem for the Laplace operator.

4. Evaluation of the explicit terms

To complete the description of the algorithm for the spectral simulation of incompressible flows it is necessary to show how the explicit terms of the equations are evaluated. In the momentum equation two terms, the pressure gradient and the nonlinear term, must be considered, while in the pressure Poisson equation only a divergence term must be evaluated. In the proposed method all these terms, expressed in weak form, are calculated by a pseudospectral technique, which requires to introduce the following sets of points along the three spherical "directions":

$$r_g = ((1+s_g)/2)^{1/2}, \quad g = 1,\dots,N+1, \tag{4.1}$$

$$\theta_h = \cos^{-1} z_h, \quad h = 1,\dots,N+2, \tag{4.2}$$

$$\phi_k = \frac{\pi(k-1)}{N}, \quad k = 1,\dots,2N, \tag{4.3}$$

where s_g are the $(0,\frac{1}{2})$ Gauss–Jacobi quadrature points over the interval $|s| \leqslant 1$ and z_h are the Gauss–Legendre points over the interval $|z| \leqslant 1$. The pseudospectral technique amounts to the following two steps:

1. compute the point values of the required term (gradient, divergence, nonlinear);
2. L^2_w project, with $w = \sin\theta$, the term on the basis functions by Fourier transform and Gaussian quadrature.

The two steps are performed by standard techniques, so that it will suffice to give here only the essential elements required by the present method, for details the reader is referred to [23].

A scalar function $u = u(r,\theta,\phi)$ defined over the sphere will be represented either by its expansion coefficients, organized in the structured three-dimensional array,

$$\boldsymbol{U} = \{u^m_{i,\ell},\ 0 \leqslant i \leqslant N-\ell,\ |m| \leqslant \ell \leqslant N,\ -N+1 \leqslant m \leqslant N\}, \tag{4.4}$$

or by the three-dimensional rectangular array

$$\boldsymbol{\mathcal{U}} = \{u(r_g,\theta_h,\phi_k),\ g = 1,\dots,N+1,\ h = 1,\dots,N+2,\ k = 1,\dots,2N\}, \tag{4.5}$$

of its point values over the aforementioned spherical grid.

The point values $\boldsymbol{\mathcal{U}}$ are computed from the expansion coefficients $\boldsymbol{U}$ by the following transformation

$$\boldsymbol{\mathcal{U}} = \mathbb{F}^{-1}(\widehat{\mathbb{P}}(\mathbb{B}(\boldsymbol{U}))), \tag{4.6}$$

where $\mathbb{F}$ denotes the Fourier transform and $\widehat{\mathbb{P}}$ and $\mathbb{B}$ amount to multiply each coefficient by the value assumed by the corresponding basis functions, normalized associated Legendre function and radial basis function respectively, on the Gauss points.

The L^2_w projection of the point values $\boldsymbol{\mathcal{U}}$ onto the basis functions requires to introduce the weights v_g of the Gauss–Jacobi quadrature formula with $N+1$ points and also w_h of the Gauss–Legendre formula with $N+2$ points. One has

$$\boldsymbol{U} = \frac{1}{4}\mathbb{B}_G(\widehat{\mathbb{P}}_G(\mathbb{F}(\boldsymbol{\mathcal{U}}))), \tag{4.7}$$

where the operators $\mathbb{B}_G$ and $\hat{\mathbb{P}}_G$ include the multiplication by the appropriate weights of the Gaussian quadrature and by the point values of the basis functions. Transformations $\widehat{\mathbb{P}}, \widehat{\mathbb{P}}_G, \mathbb{B}, \mathbb{B}_G$ are actually performed by matrix-matrix multiplications.

We analyze first the transformations needed to evaluate the nonlinear term. The transformations for vector fields in spherical coordinates are more complicated since point values are required for the *spherical components* of the velocity field, which are indicated by u_r, u_θ and u_ϕ, to give $\vec{\boldsymbol{\mathcal{U}}} = (\boldsymbol{\mathcal{U}},\boldsymbol{\mathcal{V}},\boldsymbol{\mathcal{W}}) = (\boldsymbol{\mathcal{U}}_r,\boldsymbol{\mathcal{U}}_\theta,\boldsymbol{\mathcal{U}}_\phi)$, whereas the structured arrays of the expansion coefficients are known for the *uncoupled components* u_1, u_2 and u_3, denoted collectively as $\vec{\boldsymbol{U}} = (\boldsymbol{U}_1,\boldsymbol{U}_2,\boldsymbol{U}_3)$. These two sets of vector components are related by the transformation operator Θ defined in Section 3, which is acting in the space of the Fourier coefficients of the velocity components. By taking into account the role of the uncoupling transformations $\boldsymbol{\Theta}$ and $\boldsymbol{\Theta}_0$, the transformations for the velocity vector variable and the L^2_w projection of the nonlinear term will be indicated formally as

$$\vec{\boldsymbol{\mathcal{U}}} = \mathbb{F}^{-1}(\Theta^{-1}(\widehat{\mathbb{P}}(\mathbb{B}(\vec{\boldsymbol{U}})))) \quad \text{and} \quad \vec{\boldsymbol{N}} = \frac{1}{4}\mathbb{B}_G(\widehat{\mathbb{P}}_G(\Theta(\mathbb{F}(\vec{\boldsymbol{\mathcal{N}}})))), \tag{4.8}$$

respectively. The evaluation of the nonlinear term $(\boldsymbol{u}\cdot\nabla)\boldsymbol{u}$ in weak form proceeds as follows. First, transform the expansion coefficients $\vec{\boldsymbol{U}}$ of the uncoupled velocity components to the values $\vec{\boldsymbol{\mathcal{U}}}$ of the spherical components in the physical space by means of $\vec{\boldsymbol{\mathcal{U}}} = \mathbb{F}^{-1}(\Theta^{-1}(\widehat{\mathbb{P}}(\mathbb{B}(\vec{\boldsymbol{U}}))))$. Second, evaluate the derivatives $\boldsymbol{\mathcal{U}}_{\partial r}, \boldsymbol{\mathcal{U}}_{\partial\theta}$ and $\boldsymbol{\mathcal{U}}_{\partial\phi}$, and similarly for the other two spherical components $\boldsymbol{\mathcal{V}}$ and $\boldsymbol{\mathcal{W}}$. This requires to know the point values of the derivative of both the radial basis functions, namely, $dB^\ell_i(r_g)/ds$, and the normalized associated Legendre functions, namely, $d\widehat{P}^{|m|}_\ell(\cos\theta_h)/d\theta$.

Then determine the spherical components of the nonlinear term $(\mathbf{u}\cdot\nabla)\mathbf{u}$ through the expressions

$$\mathcal{N}_r = \mathcal{U} \star \mathcal{U}_{\partial r} + \mathcal{R}^{-1}\mathcal{V} \star (\mathcal{U}_{\partial\theta} - \mathcal{V}) + \mathcal{R}^{-1}\mathcal{W} \star (\mathcal{U}_{\partial\phi}\mathcal{S}^{-1} - \mathcal{W}), \tag{4.9}$$

$$\mathcal{N}_\theta = \mathcal{U} \star \mathcal{V}_{\partial r} + \mathcal{R}^{-1}\mathcal{V} \star (\mathcal{V}_{\partial\theta} + \mathcal{U}) + \mathcal{R}^{-1}\mathcal{W} \star (\mathcal{V}_{\partial\phi}\mathcal{S}^{-1} - \mathcal{W}\mathcal{C}\mathcal{S}^{-1}), \tag{4.10}$$

$$\mathcal{N}_\phi = \mathcal{U} \star \mathcal{W}_{\partial r} + \mathcal{R}^{-1}\mathcal{V} \star \mathcal{W}_{\partial\theta} + \mathcal{R}^{-1}\mathcal{W} \star (\mathcal{U} + \mathcal{W}_{\partial\phi}\mathcal{S}^{-1} + \mathcal{V}\mathcal{C}\mathcal{S}^{-1}), \tag{4.11}$$

where $\star$ denotes the element-by-element multiplication of arrays and where we have introduced the diagonal matrices

$$\mathcal{R} \equiv \mathrm{diag}\,(r_g,\ g = 1,\dots,N+1), \tag{4.12}$$

$$\mathcal{S} \equiv \mathrm{diag}\,(\sin\theta_h,\ h = 1,\dots,N+2), \tag{4.13}$$

$$\mathcal{C} \equiv \mathrm{diag}\,(\cos\theta_h,\ h = 1,\dots,N+2). \tag{4.14}$$

We notice that the left multiplication by $\mathcal{R}^{-1}$ must be done on any column and for any plane $k =$ constant of the subsequent 3D array. A similar remark holds for the right multiplication by the diagonal matrices $\mathcal{S}^{-1}$ and $\mathcal{C}$. Finally evaluate the L^2_w projection of the nonlinear term by means of

$$\vec{\boldsymbol{N}} = \frac{1}{4}\mathbb{B}_G(\hat{\mathbb{P}}_G(\Theta(\mathbb{F}(\vec{\boldsymbol{\mathcal{N}}})))). \tag{4.15}$$

The evaluation of the gradient term proceeds along the same lines. From the expansion coefficients $\mathbf{P} = \{p^m_{i,\ell},\ 0 \leqslant i \leqslant N-\ell,\ |m| \leqslant \ell \leqslant N,\ -N+1 \leqslant m \leqslant N\}$ of the pressure, one first evaluates the spherical components of its gradient in the Fourier space, but at the grid points (r_g,θ_h), i.e. $\mathbb{F}^{-1}$ is omitted. Then, the transformation Θ is applied to yield the gradient components in the uncoupled basis. Finally, the term is projected to give its contribution to the momentum equation in weak form.

The divergence of velocity is evaluated by first transforming the expansion coefficients $\vec{\boldsymbol{\mathcal{U}}}$ into the values at the grid points (r_g,θ_h), and obtaining also the corresponding derivatives with respect to r and θ. Then, the transformation $\boldsymbol{\Theta}^T$ is applied to obtain the spherical velocity components and their derivatives. Finally, the expression of divergence is evaluated, paying attention that the transformation $\boldsymbol{\Theta}$ depends on θ, and projected to have the weak term contributing to the right-hand side of the scalar pressure equation.

5. Navier–stokes equations in a rotating frame

In a noninertial frame of reference the equations governing the fluid motion must be modified by including the body forces acting on the fluid as a consequence of the frame acceleration. In particular, if we consider a frame rotating with a constant angular velocity $\boldsymbol{\Omega}$ with respect to a fixed (*i.e.* inertial) system, the body force (per unit mass) consists in the Coriolis force $-2\boldsymbol{\Omega}\times\boldsymbol{u}$ plus the centrifugal force $-\boldsymbol{\Omega}\times(\boldsymbol{\Omega}\times\boldsymbol{r})$, so that the momentum equation in the noninertial frame reads

$$\frac{\partial\boldsymbol{u}}{\partial t} + (\boldsymbol{u}\cdot\nabla)\boldsymbol{u} - \nu\nabla^2\boldsymbol{u} + \nabla p = -2\boldsymbol{\Omega}\times\boldsymbol{u}, \tag{5.1}$$

since the centrifugal term has been incorporated in the reduced pressure variable p defined by

$$p(\boldsymbol{r},t) = \frac{P(\boldsymbol{r},t)}{\bar{\rho}} - \frac{1}{2}|\boldsymbol{\Omega}\times\boldsymbol{r}|^2. \tag{5.2}$$

When the rotation speed of the reference frame grows, the Coriolis term on the right hand side of the momentum equation becomes increasingly important so that taking into account the Coriolis term explicitly could lead to instabilities of the numerical scheme for high rotation speeds and to time step constraints [24]. In this section it is shown an original technique to take into account the Coriolis term implicitly and efficiently in the vector Helmholtz solver thus avoiding any unnecessary time step restriction.

5.1. Coriolis term in the uncoupled basis

Taking the z axis of the spherical coordinate system in the same direction of $\boldsymbol{\Omega}$ entails $\boldsymbol{\Omega} = \Omega\hat{\boldsymbol{z}}$, where $\hat{\boldsymbol{z}}$ is the unit vector along z. By expressing $\hat{\boldsymbol{z}}$ in terms of unit vectors of the spherical coordinate system, $\boldsymbol{\Omega} = \Omega(\cos\theta\,\hat{\boldsymbol{r}} - \sin\theta\,\hat{\boldsymbol{\theta}})$, the vector product $\boldsymbol{\Omega}\times\boldsymbol{u}$ of the Coriolis term assumes the form

$$\boldsymbol{\Omega}\times\boldsymbol{u} = \Omega(\cos\theta\,\hat{\boldsymbol{r}} - \sin\theta\,\hat{\boldsymbol{\theta}})\times(u_r\hat{\boldsymbol{r}} + u_\theta\hat{\boldsymbol{\theta}} + u_\phi\hat{\boldsymbol{\phi}}) = \Omega[-\sin\theta\,u_\phi\hat{\boldsymbol{r}} - \cos\theta\,u_\phi\hat{\boldsymbol{\theta}} + (\sin\theta\,u_r + \cos\theta\,u_\theta)\hat{\boldsymbol{\phi}}]. \tag{5.3}$$

Written as a column vector, we have:

$$\boldsymbol{\Omega}\times\boldsymbol{u} = \begin{pmatrix}\Lambda_r\\ \Lambda_\theta\\ \Lambda_\phi\end{pmatrix} = \Omega\begin{pmatrix}-\sin\theta\,u_\phi\\ -\cos\theta\,u_\phi\\ \sin\theta\,u_r + \cos\theta\,u_\theta\end{pmatrix}. \tag{5.4}$$

To obtain the representation of the Coriolis term above in the basis of the uncoupled components discussed in Section 3, we have to apply the transformation $\boldsymbol{\Theta}$ to the Fourier components with $m \neq 0$ of the Coriolis term, namely to the vector

$$\boldsymbol{\Omega} \times \boldsymbol{u}^m = \begin{pmatrix} \Lambda_r^m \\ \Lambda_\theta^m \\ \Lambda_\phi^{-m} \end{pmatrix} = \Omega \begin{pmatrix} -\sin\theta\, u_\phi^m \\ -\cos\theta\, u_\phi^m \\ \sin\theta\, u_r^{-m} + \cos\theta\, u_\theta^{-m} \end{pmatrix}. \tag{5.5}$$

The representation of the Coriolis term in the basis of the uncoupled components is therefore

$$\boldsymbol{\Theta}[\boldsymbol{\Omega} \times \boldsymbol{u}^m] = \boldsymbol{\Theta} \begin{pmatrix} \Lambda_r^m \\ \Lambda_\theta^m \\ \Lambda_\phi^{-m} \end{pmatrix} = \frac{\Omega}{\sqrt{2}} \begin{pmatrix} \sin\theta\, u_r^{-m} + \cos\theta\, u_\theta^{-m} - u_\phi^m \\ 0 \\ -\sin\theta\, u_r^{-m} - \cos\theta\, u_\theta^{-m} - u_\phi^m \end{pmatrix}. \tag{5.6}$$

Expressing this term as a function of the uncoupled components $\breve{\boldsymbol{u}}^m = (u_1^m, u_2^m, u_3^m)$ of velocity gives:

$$\boldsymbol{\Theta}[\boldsymbol{\Omega} \times (\boldsymbol{\Theta}^T \breve{\boldsymbol{u}}^m)] = \Omega \begin{pmatrix} u_3^{-m+1} \\ 0 \\ -u_1^{-m-1} \end{pmatrix}. \tag{5.7}$$

For the first Fourier mode $m = 0$, the transformation is $\boldsymbol{\Theta}_0$ and we can compute

$$\boldsymbol{\Theta}_0(\boldsymbol{\Omega} \times \boldsymbol{u}^0) = \boldsymbol{\Theta}_0 \begin{pmatrix} \Lambda_r^0 \\ \Lambda_\theta^0 \\ \Lambda_\phi^0 \end{pmatrix} = \Omega \begin{pmatrix} -u_\phi^0 \\ 0 \\ \sin\theta\, u_r^0 + \cos\theta\, u_\theta^0 \end{pmatrix}, \tag{5.8}$$

namely, making explicit the dependence on the uncoupled components $\breve{\boldsymbol{u}}^m$ of the Fourier modes with $m = -1$ and $m = 1$:

$$\boldsymbol{\Theta}_0[\boldsymbol{\Omega} \times (\boldsymbol{\Theta}_0 \breve{\boldsymbol{u}}^0)] = \Omega \begin{pmatrix} -u_3^1 \\ 0 \\ u_1^{-1} \end{pmatrix}. \tag{5.9}$$

To see the contribution of the Coriolis term to the weak vector equations, let us remind the spectral expansion of the first uncoupled component $u_1^{m-1}(r,\theta)$:

$$u_1^{m-1}(r,\theta) = \sum_{\ell=|m-1|}^{N} u_\ell^{m-1;1}(r)\, \widehat{P}_\ell^{|m-1|}(\cos\theta) = \sum_{\ell=|m-1|}^{N} \left[\sum_{i=0}^{N-\ell} u_{\ell;i}^{m-1;1}\, B_i^\ell(r) \right] \hat{P}_\ell^{|m-1|}(\cos\theta). \tag{5.10}$$

The expansion of the first uncoupled component of the Coriolis force is similar and yields

$$u_3^{-m+1}(r,\theta) = \sum_{\ell=|m-1|}^{N} \left[\sum_{i=0}^{N-\ell} u_{\ell;i}^{-m+1;3}\, B_i^\ell(r) \right] \widehat{P}_\ell^{|m-1|}(\cos\theta). \tag{5.11}$$

The Coriolis contribution to the weak discrete equation is obtained by multiplying $u_3^{-m+1}(r,\theta)$ by the weighting function $Q_{i'}^{\ell}(s)\, \widehat{P}_{\ell'}^{|m-1|}(\cos\theta)$ and by the dimensionless spherical metric factor $r^2 \sin\theta = \frac{1+s}{2} \sin\theta$ and integrating over the variables s and θ. A direct calculation yields

$$u_3^{-m+1}(r,\theta) \to M_{[\ell]}\, u_{[\ell]}^{-m+1;3}, \tag{5.12}$$

where matrix $M_{[\ell]}$ has been defined in (3.20) and the arrays $u_{[\ell]}^{m;1,2,3}$ are defined, as usual, by

$$u_{[\ell]}^{m;1,2,3} \equiv \{ u_{[\ell]\, i}^{m;1,2,3},\ 0 \leqslant i \leqslant N - \ell \} \quad \text{for } |m| \leqslant \ell \leqslant N. \tag{5.13}$$

The calculation of the Coriolis contribution to the third component of the weak uncoupled equation is analogous. Thus, the vector quantity proportional to the contribution due to Coriolis force to the weak equation for the any generic mode with $\ell > 0$ and $m \neq 0$, and for the single special mode with $\ell = 0$ and $m = 0$, are, respectively,

$$\begin{pmatrix} \Omega M_{[\ell]}\, u_{[\ell]}^{-m+1;3} \\ 0 \\ -\Omega M_{[\ell]}\, u_{[\ell]}^{-m-1;1} \end{pmatrix} \quad \text{and} \quad \begin{pmatrix} -\Omega M_{[0]}\, u_{[0]}^{1;3} \\ 0 \\ \Omega M_{[0]}\, u_{[0]}^{-1;1} \end{pmatrix}. \tag{5.14}$$

The exchange of sign in the components of the special mode with respect to any other mode must be noticed.

5.2. Elliptic system with Coriolis coupling

The Coriolis term is now added to the momentum equation and taken into account in an implicit manner, to give:

$$(-\nabla^2 + \boldsymbol{\alpha} \times + \gamma)\boldsymbol{u} = \boldsymbol{f}(\boldsymbol{r}), \tag{5.15}$$

where $\boldsymbol{\alpha} = 2\nu^{-1}\boldsymbol{\Omega}$ and $\gamma = 1/(\nu\Delta t)$. By recalling the uncoupled form of the Helmholtz equation of the time-discretized problem discussed in Section 3, the first and third components of each spectral mode with $m \neq 0$ lead to the two equations

$$A_{[\ell]}\, u_{[\ell]}^{m-1;1} + \alpha M_{[\ell]}\, u_{[\ell]}^{-(m-1);3} = f_{[\ell]}^{m-1;1}, \tag{5.16}$$

$$A_{[\ell]}\, u_{[\ell]}^{m+1;3} - \alpha M_{[\ell]}\, u_{[\ell]}^{-(m+1);1} = f_{[\ell]}^{m+1;3}, \tag{5.17}$$

where $A_{[\ell]} = D_{[\ell]} + \gamma M_{[\ell]}$. In the two equations above there are four different unknowns, namely $u_{[\ell]}^{m-1;1}$, $u_{[\ell]}^{-(m-1);3}$, $u_{[\ell]}^{m+1;3}$ and $u_{[\ell]}^{-(m+1);1}$. On the other hand, the index m can assume positive and negative values, so that we can consider the two equations with $m \geqslant 0$ and derive the equation pair corresponding to negative m by replacing m with $-m$. In this way we obtain the other two equations

$$A_{[\ell]}\, u_{[\ell]}^{-(m+1);1} + \alpha M_{[\ell]}\, u_{[\ell]}^{m+1;3} = f_{[\ell]}^{-(m+1);1}, \tag{5.18}$$

$$A_{[\ell]}\, u_{[\ell]}^{-(m-1);3} - \alpha M_{[\ell]}\, u_{[\ell]}^{m-1;1} = f_{[\ell]}^{-(m-1);3}. \tag{5.19}$$

We now note that the first Eq. (5.16) of the first pair has the same unknowns, $u_{[\ell]}^{m-1;1}$ and $u_{[\ell]}^{-(m-1);3}$, of the second Eq. (5.19) of the second pair: thus we can write the following system of two coupled equations

$$\begin{cases} A_{[\ell]}\, u_{[\ell]}^{m-1;1} + \alpha M_{[\ell]}\, u_{[\ell]}^{-(m-1);3} = f_{[\ell]}^{m-1;1}, \\ -\alpha M_{[\ell]}\, u_{[\ell]}^{m-1;1} + A_{[\ell]}\, u_{[\ell]}^{-(m-1);3} = f_{[\ell]}^{-(m-1);3}. \end{cases} \tag{5.20}$$

Setting $m - 1 \to m$, this system can be written more simply as

$$\begin{cases} A_{[\ell]}\, u_{[\ell]}^{m;1} + \alpha M_{[\ell]}\, u_{[\ell]}^{-m;3} = f_{[\ell]}^{m;1}, \\ -\alpha M_{[\ell]}\, u_{[\ell]}^{m;1} + A_{[\ell]}\, u_{[\ell]}^{-m;3} = f_{[\ell]}^{-m;3}. \end{cases} \tag{5.21}$$

In a similar way, the second Eq. (5.17) of the first pair has the same unknowns, $u_{[\ell]}^{m+1;3}$ and $u_{[\ell]}^{-(m+1);1}$, of the first Eq. (5.18) of the second pair, so that we can write a second system of two coupled equations

$$\begin{cases} A_{[\ell]}\, u_{[\ell]}^{-m;1} + \alpha M_{[\ell]}\, u_{[\ell]}^{m;3} = f_{[\ell]}^{-m;1} \\ -\alpha M_{[\ell]}\, u_{[\ell]}^{-m;1} + A_{[\ell]}\, u_{[\ell]}^{m;3} = f_{[\ell]}^{m;3} \end{cases} \tag{5.22}$$

The two systems are characterized by the same matrices so that they can be considered altogether by letting m running in the interval $[-N+1, N-1]$, but skipping the value $m = -1$, which corresponds to the special mode characterized by the just mentioned sign exchange in the components 1 and 3.

After including the possibly nonhomogeneous Dirichlet boundary conditions, the system is lifted to

$$\begin{cases} A_{[\ell]}\, u_{[\ell]}^{m;1} + \alpha M_{[\ell]}\, u_{[\ell]}^{-m;3} = g_{[\ell]}^{m;1} \\ -\alpha M_{[\ell]}\, u_{[\ell]}^{m;1} + A_{[\ell]}\, \mathrm{u}_{[\ell]}^{-m;3} = g_{[\ell]}^{-m;3} \end{cases} \tag{5.23}$$

where all the matrices are the lifted counterparts of the matrices pertaining to all modes, for instance:

$$\mathrm{A}_{[\ell]} = \mathrm{D}_{[\ell]} + \gamma \mathrm{M}_{[\ell]}, \tag{5.24}$$

and the right-hand sides $g_{[\ell]}^{m;1}$ and $g_{[\ell]}^{-m;3}$ are the lifted counterpart of $f_{[\ell]}^{m;1}$ and $f_{[\ell]}^{-m;3}$, including the effect of nonzero boundary condition. This system can be written also as follows:

$$\begin{pmatrix} A_{[\ell]} & +\alpha M_{[\ell]} \\ -\alpha M_{[\ell]} & A_{[\ell]} \end{pmatrix} \begin{pmatrix} u_{[\ell]}^{m;1} \\ u_{[\ell]}^{-m;3} \end{pmatrix} = \begin{pmatrix} g_{[\ell]}^{m;1} \\ g_{[\ell]}^{-m;3} \end{pmatrix}. \tag{5.25}$$

Let us now reorder the equations and the unknowns by writing the components 1 and 3 of each radial mode consecutively, and introduce the reordered vector of the unknowns

$$\mathbf{u}_{[\ell]}^{m} \equiv \{\mathrm{u}_{[\ell]\,1}^{m;1}, \mathrm{u}_{[\ell]\,1}^{-m;3},\ \mathrm{u}_{[\ell]\,2}^{m;1}, \mathrm{u}_{[\ell]\,2}^{-m;3},\ \ldots,\ \mathrm{u}_{[\ell]\,N-\ell}^{m;1}, \mathrm{u}_{[\ell]\,N-\ell}^{-m;3}\} \tag{5.26}$$

and similarly for the right-hand side $\boldsymbol{g}_{[\ell]}^{m}$. By virtue of the new ordering, the coupled system of two equations for $\mathrm{u}_{[\ell]}^{m;1}$ and $\mathrm{u}_{[\ell]}^{-m;3}$, for $\ell = m-1, m, m+1, \ldots, N$, translates into a linear system with a 2×2-block tridiagonal profile for the new unknown $\mathbf{u}_{[\ell]}^{m}$

$$\mathbf{B}_{[\ell]}\, \mathbf{u}_{[\ell]}^{m} = \boldsymbol{g}_{[\ell]}^{m}, \tag{5.27}$$

where $\mathbf{B}_{[\ell]}$ is a nonsymmetric matrix of order $2(N - \ell + 1)$ and with a bandwidth of $2 \times 3 = 6$.

The system corresponding to the special mode ± 1 is

$$\begin{cases} A_{[0]}\, u_{[0]}^{-1;1} - \alpha M_{[0]}\, u_{[0]}^{1;3} = g_{[0]}^{-1;1} \\ \alpha M_{[0]}\, u_{[0]}^{-1;1} + A_{[0]}\, u_{[0]}^{1;3} = g_{[0]}^{1;3} \end{cases} \tag{5.28}$$

One introduces the unknown with reordered components, as follows

$$\mathbf{u}_{[0]} \equiv \{u_{[0]\,1}^{-1;1}, u_{[0]\,1}^{1;3},\ u_{[0]\,2}^{-1;1}, u_{[0]\,2}^{1;3},\ \ldots,\ u_{[0]\,N}^{-1;1}, u_{[0]\,N}^{1;3}\} \tag{5.29}$$

and similarly for the right-hand side $\boldsymbol{g}_{[0]}$. Therefore, the special system for the particular mode ± 1 is

$$\tilde{\mathbf{B}}_{[0]}\, \mathbf{u}_{[0]} = \boldsymbol{g}_{[0]}, \tag{5.30}$$

where the off-diagonal blocks of matrix $\tilde{\mathbf{B}}_{[0]}$ have opposite signs with respect to those of matrices $\mathbf{B}_{[\ell]}$, with $\ell > 0$. The solution of this system can be obtained using matrix $\mathbf{B}_{[0]}$ by changing the sign of the second component of the source and of the solution.

6. Numerical results

To test the spectral solvers for the Navier–Stokes equations in a sphere, the exact solution must be infinitely differentiable throughout the computational domain, including the sphere center. This can be easily achieved by defining the pressure and velocity fields as a function of the Cartesian coordinates and in terms of the Cartesian components. As far as the error of the numerical solution is concerned, we measure the errors in terms of L_w^2 norm, with weight $w = r^2 \sin\theta$. In particular the norm of a vector function represented in spherical components is defined in the standard way

$$\|\boldsymbol{u}\|_{L_w^2}^2 = \|u_r\|_{L_w^2}^2 + \|u_\theta\|_{L_w^2}^2 + \|u_\phi\|_{L_w^2}^2.$$

6.1. Spatial convergence and LBB condition

The spatial accuracy of the proposed spectral approximation is verified against the exact analytical solution to the steady state Navier–Stokes equations defined by the following velocity and pressure fields, expressed in Cartesian coordinates, as follows:

$$\begin{aligned} u_x^{\mathrm{e}}(x,y,z) &= (\sin x)(\cos y)(\sin z) \\ u_y^{\mathrm{e}}(x,y,z) &= (\cos x)(\sin y)(\sin z) \\ u_z^{\mathrm{e}}(x,y,z) &= 2(\cos x)(\cos y)(\cos z) \\ p^{\mathrm{e}}(x,y,z) &= 3(\cos x)(\cos y)(\cos z) \end{aligned}$$

The velocity field above is solenoidal but the steady-state momentum equation has a nonzero source term given by $\boldsymbol{f}(\boldsymbol{r}) = -\nabla^2 \boldsymbol{u}^{\mathrm{e}} + \nabla p^{\mathrm{e}} + \mathrm{Re}(\boldsymbol{u}^{\mathrm{e}} \cdot \nabla)\boldsymbol{u}^{\mathrm{e}}$, to be added to its right-hand side. The vector field $\boldsymbol{f}(\boldsymbol{r})$ is easily evaluated in Cartesian form and then transformed in spherical components. The spectral solver is run to produce the steady state numerical solution in a sphere of radius $a = 8$ for the Reynolds number $\mathrm{Re} = 10$. In Fig. 2 the velocity and pressure errors in the L_w^2 norm of the computed solutions for different spectral resolutions with $N = 20, 25, 30$ and 35 are reported.

The figure contains the spatial convergence rate of two implementations of the solver with different spectral approximation of the pressure field. In fact, for the incompressible equations the spatial discretization of the pressure is known to be subject to a stability constraint, called LBB condition. When this condition is violated, spurious pressure modes appear in the computed pressure field. Moreover, for spatial discretization of local type, such as finite elements or differences, unphysical spatial oscillations are generated also in the velocity field, provided the time-step is sufficiently small [25].

The situation is slightly different for approximations of global type, such as the spectral method, of interest here. It has been shown in [26] for Galerkin–Legendre approximations to the Cartesian Navier–Stokes equations that the violation of LBB condition produces spurious spatial oscillations, but only in the pressure field while the convergence of the velocity is unaffected. In any case the development of spurious pressure modes is prevented in the spectral solution simply by using a polynomial representation for the pressure of two degree lower than that used for the velocity. This treatment must be adopted for the spatial discretization in each space direction with two boundary conditions.

In the present case of spherical domain, with only one non-periodic direction, the LBB condition is violated when choosing the same basis to represent the radial dependence of both velocity and pressure. The modification in the radial expansion in Jacobi polynomials consists in reducing the dimension of only the mode $m = 0, \ell = 0$, which is the subspace of functions independent of θ and ϕ. This is easily obtained by eliminating the highest mode of this subspace. The modified expansion of the pressure field including the order reduction to satisfy the LBB stability condition in the radial direction would be as in the complete expression (3.27) but for the first term of the expansion, corresponding to $m = 0$ and $\ell = 0$, which is replaced by the following reduced series

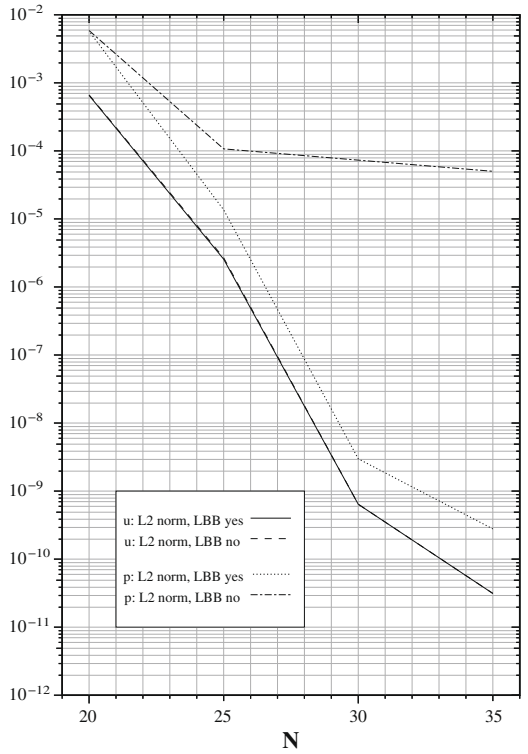

Fig. 2. Convergence rate of the spatial discretization error. The two velocity errors are nearly identical and the corresponding curves are almost indistinguishable in the plot.

$$\frac{1}{\sqrt{2}}\sum_{i=0}^{N-1} p_{i;0}^{0} B_i^0(r), \tag{6.1}$$

where the occurrence of -1 in the upper extreme of the sum must be noticed and where we have used $\widehat{P}_0^0 = 1/\sqrt{2}$. Fig. 2 shows the convergence curves of the velocity and pressure errors for the solver with Jacobi polynomials of equal order for $\boldsymbol{u}$ and p, violating the LBB condition, and for the solver with a pressure polynomial one degree less than that of velocity, thus respecting the LBB condition. The curves show the lack of convergence of pressure of the equal order approximation and also that the velocity solution is equally accurate and convergent irrespective of the fulfillment of the LBB condition, similarly to the result established and verified for the Cartesian case in [26].

To illustrate the nature of the pressure spurious modes in the spherical problem, in Fig. 3 the spatial distribution of the pressure difference between the numerical and the exact solutions is reported for $N = 30$ in one quarter of the circle of radius $a = 5$ on the plane $\phi = 0$. These oscillations are found symmetric with respect to the sphere centre and therefore the plot is representative of the situation of the pressure field throughout the sphere.

In Fig. 4 we report the pressure difference of the solution produced by the solver respecting the LBB condition according to the reduced expansion in (6.1). The left plot gives the level curves of pressure error while the right plot gives its 3D representation. The complete elimination of the spatial oscillations can be appreciated together with a concomitant reduction of the error by six orders of magnitude.

6.2. Time convergence

The time accuracy of the second-order BDF scheme is verified by comparison with an exact solution to the time-dependent Navier–Stokes equations. Consider first the stationary 2D velocity field

$$u_x^s(x,z) = -\cos x \sin z,$$
$$u_z^s(x,z) = \sin x \cos z,$$

which is solenoidal. The time-dependent velocity field solution to the unsteady 2D Navier–Stokes equations and the corresponding source term are given by

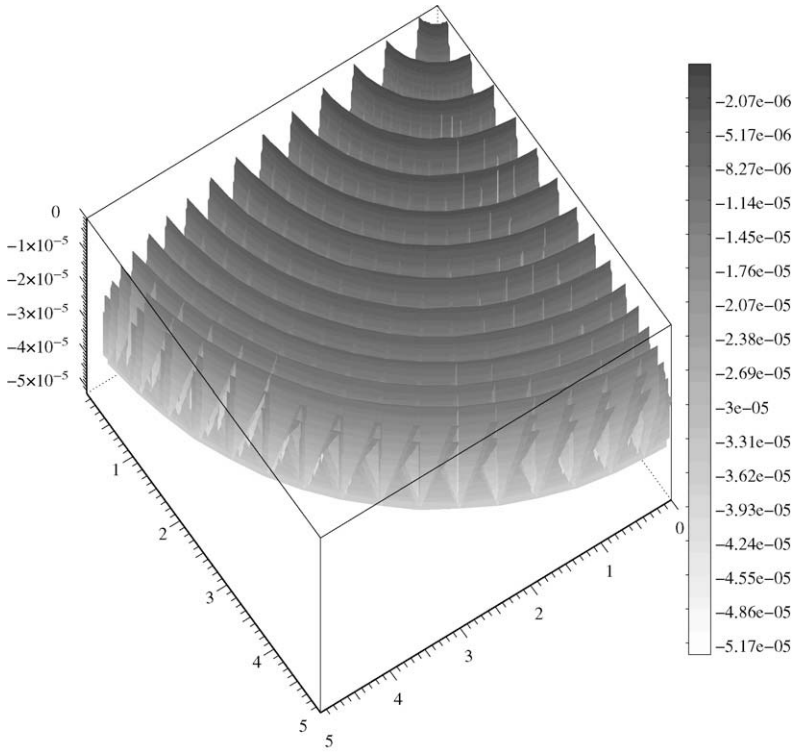

Fig. 3. Spurious pressure modes of the steady solution for Re = 10 with $N = 30$. Only a quarter of the circle of radius $a = 5$ on the plane $\phi = 0$ is shown.

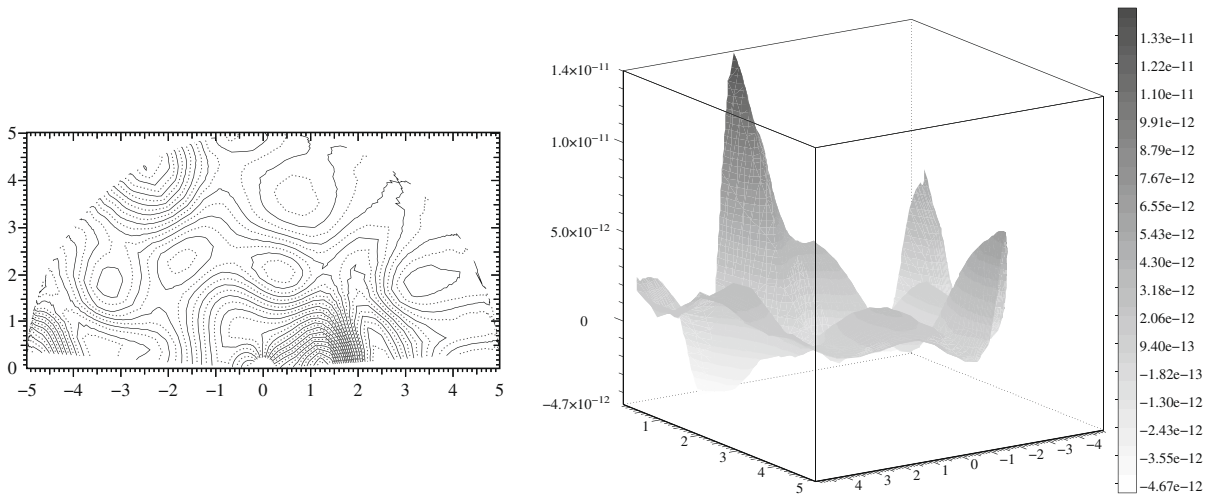

Fig. 4. Pressure error of the method satisfying LBB stability condition by elimination of the highest Jacobi polynomial in pressure radial expansion. Steady solution for Re = 10 with $N = 30$ in the half circle of radius $a = 5$ on the half plane $\phi = 0,\ x > 0$.

$$\boldsymbol{u}(x,z,t) = \boldsymbol{u}^{s}(x,z)g(t),$$
$$\boldsymbol{f}(x,z,t) = \boldsymbol{u}^{s}(x,z)\left[g'(t) + \frac{2g(t)}{\mathrm{Re}}\right].$$

The pressure field of this time-dependent solution is given by

$$p(x,z,t) = -\frac{1}{4}[\cos(2x) + \cos(2z)]g^2(t),$$

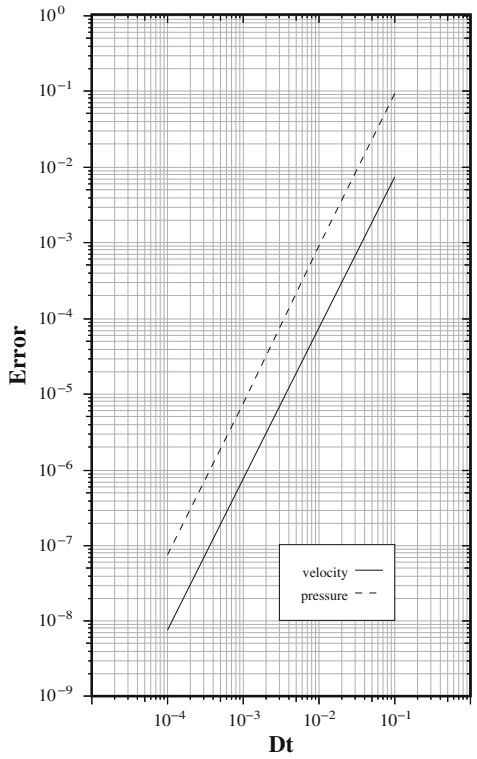

Fig. 5. Convergence rate of the time discretization error in $l^\infty(0,T;L^2)$ norm, for $N = 30$.

where we assume $g(t) = \sin^2 t$. This Cartesian velocity field in the vertical plane $x - z$ is transformed in its 3D counterpart in spherical components u_r, u_θ and u_ϕ to test the Navier–Stokes spectral solver inside a sphere. The velocity boundary values are determined from the exact solution as $\boldsymbol{b}(\theta,\phi,t) = \boldsymbol{u}(a,\theta,\phi,t)$. Similarly, the initial velocity field is taken as $\boldsymbol{u}_0(\boldsymbol{r}) = \boldsymbol{u}(\boldsymbol{r},0) = \boldsymbol{u}^s(\boldsymbol{r})\,g(0) = 0$. Finally, the initial pressure field required by the second-order incremental BDF scheme is taken as $p_0(\boldsymbol{r}) = p(\boldsymbol{r},0) = 0$. The exact solution for $\mathrm{Re} = 10$ is assumed and the domain is taken the sphere of radius $a = 5$. The temporal convergence is measured in the norm $l^\infty(0,T;L^2)$.

Fig. 5 shows the decrease of the $l^\infty(1,2;L^2)$ error of velocity and pressure when the step-size Δt decreases from $\Delta t = 0.01$ to $\Delta t = 10^{-4}$. The second-order accuracy of the solution algorithm is clearly confirmed.

6.3. Helmholtz–Coriolis solver

To verify the correctness of the spectral elliptic solver for the vector problem with the Coriolis term taken into account implicitly, we have considered an analytical test built on an exact solution consisting of the vector field defined in terms of its Cartesian components:

$$u_x = e^{c_1(x-x_1)^2 + d_1(y-y_1)^2 + z - z_1}$$
$$u_y = e^{c_2(x-x_2)^2 + d_2(y-y_2)^2 + z - z_2}$$
$$u_z = e^{c_3(x-x_3)^2 + d_3(y-y_3)^2 + z - z_3}$$

with all the parameters given by

$$c_1 = 1,\ d_1 = 2,\ x_1 = 0.1,\ y_1 = 0.2,\ z_1 = 0.3;$$
$$c_2 = 2,\ d_2 = 3,\ x_2 = 0.2,\ y_2 = 0.3,\ z_2 = 0.4;$$
$$c_3 = 3,\ d_3 = 4,\ x_3 = 0.3,\ y_3 = 0.4,\ z_3 = 0.5.$$

The vector Dirichlet problem for the Helmholtz–Coriolis vector Eq. (5.15) is solved for $\gamma = 1.5$ and $\alpha = 1$ in the unit sphere $r \leqslant 1$ with the analytical solution defined above for the indicated values of c_i and d_i, for $i = 1,2,3$. The errors of the spectral solutions for different spatial resolutions are reported in Table 1. These results demonstrate the spectral convergence of the solver with an implicit account of the Coriolis term.

Table 1
Vector Dirichlet problem for Helmholtz–Coriolis operator with $\gamma = 1.5$ and $\alpha = 1$ inside the unit sphere. Exact solution: see the text.

N	L^∞ error	L^2_w error
15	6.1×10^{-2}	2.8×10^{-2}
20	4.8×10^{-4}	1.8×10^{-4}
30	2.8×10^{-9}	1.0×10^{-9}
40	8.1×10^{-12}	1.9×10^{-12}
50	8.1×10^{-12}	3.1×10^{-12}

6.4. Flow in a precessing and spinning sphere

The Navier–Stokes solver with the implicit account of the Coriolis term described in Section 5 is tested by computing the flow in a rotating and precessing sphere and comparing the computed results with the solution given by Kida an Nakayama in [14]. The fluid motion in a sphere of radius a is driven by the rotation of its surface around two orthogonal axes. The sphere is rotating around a horizontal axis with a constant spinning angular velocity Ω_s. This axis rotates around another, vertical, axis with a precession angular velocity Ω. The fluid motion is described in the precessing frame and the Cartesian coordinates (x, y, z) are taken with z axis coincident with the precession direction of $\boldsymbol{\Gamma}$ and the x axis coincident with the spinning axis of the sphere. The boundary conditions for the (dimensional) velocity of this problems are

$$\boldsymbol{u}_{|r=a} = \boldsymbol{b} = a\Omega_s \hat{\boldsymbol{x}} \times \hat{\boldsymbol{r}} = -a\Omega_s \sin\phi\, \hat{\boldsymbol{\theta}} - a\Omega_s \cos\theta \cos\phi\, \hat{\boldsymbol{\phi}}.$$

In this problem, the variables are normalized by taking a and Ω as reference of length and time, and this leads to two dimensionless control parameters

$$\mathrm{Re} = \frac{a^2\Omega_s}{\nu} \quad \text{and} \quad \boldsymbol{\Gamma} = \frac{\boldsymbol{\Omega}}{\Omega_s}.$$

The dimensionless Navier–Stokes equations assume the form

$$\frac{\partial \boldsymbol{u}}{\partial t} + 2\boldsymbol{\Gamma} \times \boldsymbol{u} - \frac{1}{\mathrm{Re}} \nabla^2 \boldsymbol{u} + \nabla p = -(\boldsymbol{u} \cdot \nabla)\boldsymbol{u}.$$

After the time discretization, the vector elliptic equation to be solved at each time step reads

$$(-\nabla^2 + 2\mathrm{Re}\boldsymbol{\Gamma} \times + \gamma)\boldsymbol{u} = \boldsymbol{f}(r, \theta, \phi),$$

where typically $\gamma = \mathrm{Re}/\Delta t$.

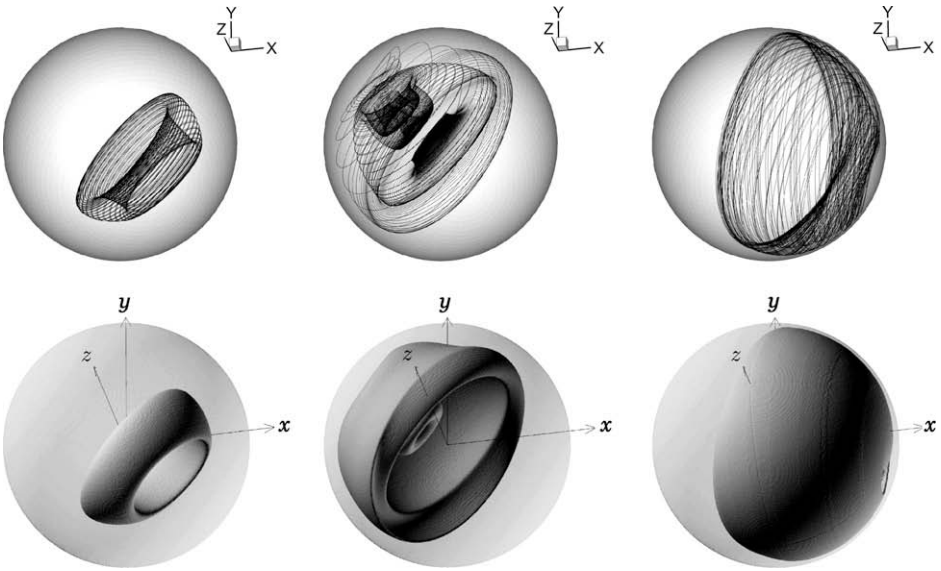

Fig. 6. Surfaces described by the streamlines passing through the points $(0, -0.57, 0)$ (left), $(-0.3, 0.30, 0)$ (center) and $(0.77, 0.5, 0)$ (right), of the steady state flow inside a rotating and precessing sphere for $\mathrm{Re} = 500$ and $\Gamma = 0.1$. Comparison of the solution computed by the present method (upper) with the solution of Kida and Nakayama [14] (lower).

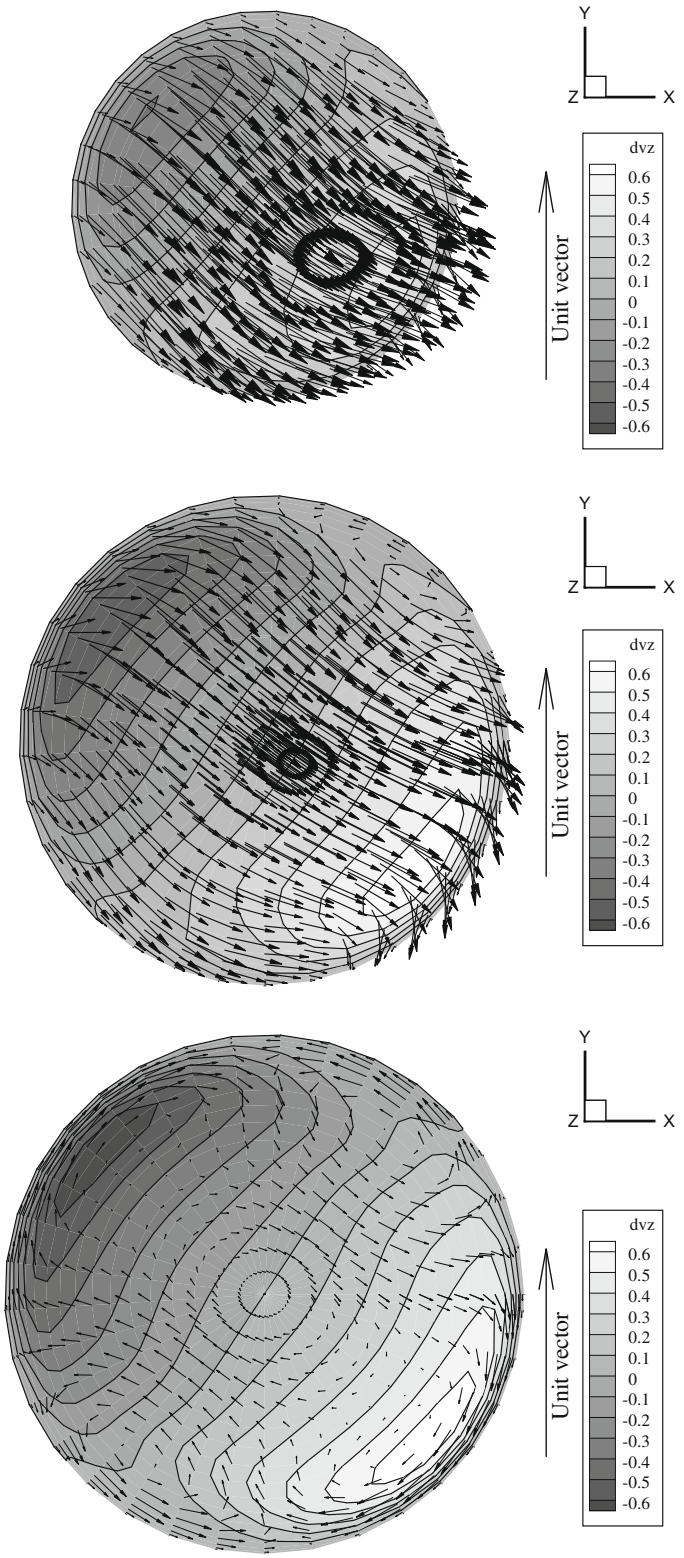

Fig. 7. Velocity in three planes normal to the z axis of precession: from top to bottom $z = -0.666, z = -0.333, z = 0$. The arrows represent the velocity difference of fluid motion with respect to the rigid rotation around the x axis with spinning angular velocity Ω_s. Contours indicate the magnitude of the z component of the velocity difference.

Steady solutions have been calculated for moderate precession velocity $\Gamma = 0.1$ by Kida and Nakayama using a spectral method based on a representation of the velocity field in terms of poloidal and toroidal potentials [14]. In the range $\mathrm{Re} \leqslant 500$, each streamline has been found to localize on a surface of toroidal shape that becomes more and more complicated as Re increases. We have compared the solution provided by the proposed spectral solver with $N = 50$ to that given in [14] for the highest value $\mathrm{Re} = 500$ considered there. The steady solution is obtained by means of the scheme with the implicit treatment of the Coriolis term using $\Delta t = 0.005$.

In Fig. 6 the three toroidal surfaces corresponding to the streamlines passing through the points (0, -0.57, 0), (-0.3, 0.30, 0) and (0.77, 0.5, 0), respectively, are compared with the surfaces given in [14]. The shape of the three surfaces is in fair agreement with the reference solution given in [14].

For a global understanding of the flow, it is convenient to describe the fluid motion in a reference system fixed with the spinning sphere boundary. This requires a plot of the vector field of the velocity difference $\boldsymbol{u} - \boldsymbol{\Omega}_s \times \boldsymbol{r}$, as done in Fig. 7 for three different planes at $z = -0.666$, $z = -0.333$ and $z = 0$. In the figure isolines of the z component of the velocity are also reported. The flow has a symmetry with respect to the sphere centre. A large circulation cell is established around a direction close to the line $x = y, z = 0$. On this main flow a secondary flow circulating about the direction $x = -y, z = 0$, perpendicular to the former, but with smaller velocity is superposed.

7. Conclusions

This work has developed a primitive-variable spectral method for simulating incompressible viscous flows inside a sphere, including the possibility of a rotating spherical container. The focus of the present effort has been to formulate a method in which the singularity of the spherical coordinates at the sphere center is coped with *ab initio* in the formulation of the spectral basis without introducing any unnecessary or even harmful over resolution near the sphere center and axis. Moreover, the aim of the work was to develop a Navier–Stokes solver as simple as possible. This objective has been reached thanks to two original components of the numerical scheme.

First, we have employed the new basis relying upon Jacobi polynomials introduced in [2] to represent radial variations of the solution of a scalar elliptic equation. In this basis the order of matrices for the radial operators decreases with the latitudinal modal index. The basis functions have been constructed so as to satisfy the regularity conditions on the expansion coefficients of spatial functions, described in terms of spherical coordinates, so that their infinite differentiability throughout the sphere is assured.

Second, we have described the unknown velocity by its spherical components but have also employed a transformation to a different set of velocity components in the Fourier space that allows a fully uncoupled solution of the vector elliptic equation. This transformation together with the properties of the associated Legendre and trigonometric functions reduces the solution of the 3D vector elliptic equation in spherical coordinates to a suitable set of fully uncoupled ordinary differential equations.

The solution of the split equations for velocity and pressure of the fractional-step projection method requires the evaluation of the gradient and divergence operators and of the nonlinear term. Since the basic unknowns in the proposed spectral method are the expansion coefficients (no collocation) and those of velocity are the uncoupled components, the evaluation of the three terms in spherical coordinates has been formulated by a simple pseudo-spectral technique.

For applications involving flows in spheres rotating around a fixed or moving axis we have also analyzed the situation of the governing equations in a noninertial reference frame rotating with a given angular velocity. We have described a modification of the velocity field solver that includes implicitly the effect of the Coriolis force on the fluid in the rotating frame. Taking into account the noninertial force in an implicit manner introduces a coupling between two of the three uncoupled velocity components. A comparison with previous numerical results has been provided that successfully checks the Navier–Stokes spectral solver in the noninertial reference frame.

In all the computed tests the correctness of the proposed solution schemes has been verified and their expected spectral convergence confirmed.

References

[1] P.W. Livermore, C.A. Jones, S.J. Worland, Spectral radial basis functions for full sphere computations, J. Comput. Phys. 227 (2007) 1209–1224.
[2] F. Auteri, L. Quartapelle, Spectral solvers for spherical elliptic problems, J. Comput. Phys. 227 (2007) 36–54.
[3] S.A. Orszag, Galerkin approximations to flows within slabs spheres and cylinders, Phys. Rev. Lett. 26 (1971) 1100–1103.
[4] P.S. Marcus, L.S. Tuckerman, Numerical simulation of spherical Couette flow. Part I: Numerical methods and steady states, J. Fluid Mech. 185 (1987) 1–30.
[5] P.S. Marcus, L.S. Tuckerman, Numerical simulation of spherical Couette flow. Part I: Transitions, J. Fluid Mech. 185 (1987) 31–65.
[6] S.K. Stanaway, B.J. Cantwell, P.R. Spalart, Navier–Stokes simulation of axisymmetric vortex rings, AIAA-88-0318, January 11-14, 1988/Reno Nevada.
[7] R.D. Moser, P. Moin, A. Leonard, A spectral numerical method for the Navier–Stokes equations with application to Taylor–Couette flows, J. Comput. Phys. 52 (1983) 524–544.
[8] G. Dumas, A. Leonard, A divergence-free spectral expansions method for three-dimensional flows in spherical-gap geometries, J. Comput. Phys. 111 (1993) 205–219.
[9] L. Quartapelle, M. Verri, On the spectral solution of the Navier–Stokes equations in spherical and cylindrical regions, Comput. Phys. Commun. 90 (1995) 1–43.
[10] Jie Shen, S. Wang, A fast and accurate numerical scheme for the primitive equations of the atmosphere, SIAM J. Numer. Anal. 36 (1999) 719–737.
[11] Jie Shen, Efficient spectral–Galerkin methods. IV. Spherical geometries, SIAM J. Sci. Comput. 20 (1999) 1438–1455.

[12] P.D. Mininni, D.C. Montgomery, Magnetohydrodynamic activity inside a sphere, Phys. Fluids 18 (2006) 116602.
[13] Ben-Yu Guo, Wei Huang, Mixed Jacobi-spherical harmonics spectral method for the Navier–Stokes equations, Appl. Numer. Math. 57 (2007) 939–961.
[14] S. Kida, K. Nakayama, Helical flow structure in a precessing sphere, J. Phys. Soc. Jpn. 77 (2008) 054401–054409.
[15] C. Egbers, G. Pfister (Eds.), Physics of Rotating Fluids, Lecture Notes in Physics, vol. 549, Springer Verlag, Berlin Heidelberg, 2000.
[16] F. Auteri, N. Parolini, A mixed-basis spectral projection method, J. Comput. Phys. 175 (2002) 1–23.
[17] F. Auteri, N. Parolini, L. Quartapelle, Simulation of 3D Flows in the Singular Driven Cavity, Report DIA SR 06-08, Politecnico di Milano, Italy, 2006.
[18] J.-L. Guermond, L. Quartapelle, Calculation of incompressible viscous flows by an unconditionally stable projection FEM, J. Comput. Phys. 132 (1997) 12–33.
[19] J.-L. Guermond, L. Quartapelle, On the approximation of the unsteady Navier–Stokes equations by finite element projection methods, Numer. Math. 80 (1998) 207–238.
[20] J.-L. Guermond, Un résultat de convergence d'ordre deux en temps pour l'approximation des équations de Navier–Stokes par une méthode de projection incrémentale, Modél. Math. Anal. Numér. (M^2AN) 33 (1999) 169–189.
[21] J.-L. Guermond, P. Minev, J. Shen, An overview of projection methods for incompressible flows, Comput. Meth. Appl. Mech. Eng. 195 (2006) 6011–6045.
[22] M. Frigo, S.G. Johnson, The design and implementation of FFTW3, Proceedings of the IEEE 93 (2005) 216–231.
[23] F. Auteri, L. Quartapelle, Navier–Stokes Spectral Solver in a Sphere, Scientific Report DIA SR-08-13, Politecnico di Milano, Dipartimento di Ingegneria Aerospaziale, 2008.
[24] R. Hollerbach, A spectral solution of the magneto-convection equations in spherical geometry, Int. J. Numer. Meth. Fluids 32 (2000) 773–797.
[25] J.-L. Guermond, L. Quartapelle, On the stability and convergence of projection methods based on Poisson pressure equation, Int. J. Numer. Meth. Fluids 26 (1998) 1039–1053.
[26] F. Auteri, J.-L. Guermond, N. Parolini, Role of LBB condition in weak spectral projection methods, J. Comput. Phys. 174 (2001) 405–420.